Auger recombination in narrow gap HgCdTe/CdHgTe quantum well heterostructures

Vladimir y Aleshkin, Vladimir Rumyantsev, Konstantin E Kudryavtsev, Alexander Dubinov, Vladimir V Utochkin, Mikhail Fadeev, Georgy Alymov, Nikolay N Mikhailov, Sergey A Dvoretsky, Frédéric Teppe, et al.

Journal of Applied Physics

Auger recombination in narrow gap HgCdTe/CdHgTe quantum well heterostructures

Cite as: J. Appl. Phys. **129**, 133106 (2021); https://doi.org/10.1063/5.0046983
Submitted: 09 February 2021 . Accepted: 22 March 2021 . Published Online: 07 April 2021

V. Ya. Aleshkin, V. V. Rumyantsev, K. E. Kudryavtsev, A. A. Dubinov, V. V. Utochkin, M. A. Fadeev, G. Alymov, N. N. Mikhailov, S. A. Dvoretsky, F. Teppe, V. I. Gavrilenko, and S. V. Morozov

Journal of Applied Physics ARTICLE scitation.org/journal/jap

Auger recombination in narrow gap HgCdTe/CdHgTe quantum well heterostructures

Cite as: J. Appl. Phys. **129**, 133106 (2021); doi: 10.1063/5.0046983
Submitted: 9 February 2021 · Accepted: 22 March 2021 ·
Published Online: 7 April 2021

V. Ya. Aleshkin,[1,2,a)] V. V. Rumyantsev,[1,2] K. E. Kudryavtsev,[1,b)] A. A. Dubinov,[1,2] V. V. Utochkin,[1,2] M. A. Fadeev,[1,2] G. Alymov,[3] N. N. Mikhailov,[4] S. A. Dvoretsky,[4] F. Teppe,[5] V. I. Gavrilenko,[1] and S. V. Morozov[1,2]

AFFILIATIONS

[1]Institute for Physics of Microstructures of RAS, 603950 Nizhny Novgorod, Russia
[2]Lobachevsky University of Nizhny Novgorod, 603950 Nizhny Novgorod, Russia
[3]Laboratory of 2d Materials for Optoelectronics, Moscow Institute of Physics and Technology, Dolgoprudny 141700, Russia
[4]Institute of Semiconductor Physics, Siberian Branch, Russian Academy of Sciences, Prospekt Akademika Lavrent'eva 13, Novosibirsk 630090, Russia
[5]Université de Montpellier, Laboratoire Charles Coulumb F-34095, Montpellier, France

[b)]**Author to whom correspondence should be addressed:** konstantin@ipmras.ru
[a)]**E-mail:** aleshkin@ipmras.ru

ABSTRACT

We present detailed theoretical analysis of nonradiative Auger recombination in narrow-gap mercury-cadmium-telluride quantum wells (HgCdTe QWs). We suggest a microscopic model to calculate Auger recombination rates in the QWs with different Cd fraction as functions of non-equilibrium carrier density with account to the complex band dispersions and wavefunctions, degenerate carrier statistics, and screening effects. Our model is validated by the comparison of measured photoconductivity kinetics with the simulated curves. Furthermore, we use the developed calculation technique to evaluate different designs of HgCdTe/CdHgTe QWs for the far-IR emitters. In particular, we consider a series of QWs with the fixed bandgap of 40 meV (lasing wavelength about 30 μm) and find out that lasing may be favored in the QWs with moderate (6%–9%) cadmium content and not in the pure binary HgTe QWs, which is in contrast to intuitive expectations within threshold energy concept for Auger recombination. Though cadmium-free QWs do provide the highest possible Auger threshold energies, Cd-containing QWs feature much more efficient screening of Coulomb potential (and so Auger interaction) by free charge carriers. The latter effect contributes decisively into the suppression of Auger processes at low temperatures and high carrier concentrations.

INTRODUCTION

Strong Auger recombination (AR) in narrow-gap semiconductor materials is one of the primary factors hindering the development of mid- and far-infrared (IR) range interband lasers. In recent years, solid progress was demonstrated in HgCdTe-based quantum well (QW) laser structures with stimulated emission (SE) around 20 μm demonstrated in Ref. 1 and visible potential for further improvement toward longer emission wavelengths. It is generally established that the possibility of SE generation in such QWs is closely associated with a highly symmetric Dirac-like band dispersion of electrons and holes that effectively raises the AR threshold energy thus suppressing nonradiative processes.[2] There are, however, only scarce reports up to date dedicated to the studies of Auger recombination in HgTe-based QWs.[2–4] Note that scientific interest was mostly focused on the relatively wide bandgap samples (e.g., 200 meV and above in Refs. 3 and 4), while AR may exhibit significantly different features in narrow-gap QWs with a bandgap below 50–80 meV. Regarding Ref. 2, the dependence of Auger rates on the excess carrier concentration was not thoroughly discussed, which may be critical for understanding the limitations being imposed on the far-IR lasing by the concurrent AR processes. Thus, the studies of Auger recombination in narrow-gap HgCdTe QWs are far from being complete.

This work is devoted to the theoretical study of Auger recombination processes in narrow-gap HgCdTe/CdHgTe QWs. In the

first part of work, we calculate the microscopic probability of the AR depending on the charge carrier's momentum taking into account band dispersion and wavefunctions of electrons and holes, and find AR rates averaged over the carrier distribution depending on the excess carrier concentration. To test our approach, we simulate interband photoconductivity (PC) kinetics for a model HgCdTe QW and compare the result with the experimentally observed photoconductivity trace. We demonstrate the carrier relaxation controlled by the Auger process in experiments agreeing well with the calculation. In the second part, we evaluate the AR rates in a series of HgCdTe QWs with a fixed band hap energy ($E_g = 40$ meV; emission wavelength ~30 μm) depending on the excess carrier concentration and discuss QW designs optimal for laser action in the far-infrared range in terms of suppressed AR. The specific wavelength range of 30–40 μm is particularly interesting due to the fact that phonon absorption makes the operation of GaAs-based quantum cascade lasers impossible in this range.[5] Here, we only consider AR at low-temperatures (all calculations on the far-IR QWs are performed for $T = 8$ K temperature) since it obviously provides a good starting position to verify whether lasing at 30 μm wavelength and beyond from HgCdTe-based QW structures is feasible.

COMPUTATIONAL MODEL FOR THE AUGER RECOMBINATION

We used four-band Kane model to calculate the band spectra and electronic states in our CdHgTe/HgCdTe QWs under consideration. Calculations were performed for the QWs grown on the [013] crystallographic plane (since most relevant experimental studies refer to such an orientation) with account to strain effects. To simplify the model, we omitted perturbations related to inversion asymmetry and symmetry lowering at the heterointerfaces. The explicit form of the Kane Hamiltonian, as well as the method for finding the electronic states, has been published elsewhere.[6] We stick to the following assumptions for the analysis of the Auger recombination. First, we suggest that excess carriers only fill the main quantization subbands, which is justified for reasonable excitation intensities. Next, non-threshold (resonant) Auger processes that involve an electron and two holes are eliminated from the consideration since those processes can be avoided by tuning them off-resonance by varying either QW parameters or sample temperature.[7] Thus, we only analyze CCHC-type AR, which is expected to dominate in narrow-gap QWs.[2] Finally, the assumption is that the resulting electron (after the CCHC process) is being heated within the same (lowest) electronic subband. This holds due to the fact that the bandgap in the QWs under consideration (40–80 meV) is much less than the splitting between the main and excited electronic subbands in the conduction band (typically 200–300 meV). While imposing certain limitations on the applicability of the developed model to the analysis of the AR in the short- and mid-wavelength QWs, the above features greatly facilitate the calculation of Auger process probability for the QW dedicated to the far-IR spectral range.

We start with the expression for the probability of the CCHC process. For an electron with the QW in-plane (2D) wavevector $\mathbf{k}$ and quantum number s (which labels the two-dimensional subband and the spin indices), it can be written as

$$W(\mathbf{k},s)=\frac{2\pi}{\hbar}\sum_{\mathbf{k}_1,\mathbf{k}'}\sum_{s_1,s',s_f}\frac{S^2}{(2\pi)^4}\iint d^2k_1 d^2k' |V(\mathbf{k},s,\mathbf{k}_1,s_1,\mathbf{k}',s',\mathbf{k}_f,s_f)|^2 f(\mathbf{k}_1,s_1)[1-f(\mathbf{k}',s')][1-f(\mathbf{k}_f,s_f)]\times\delta(\varepsilon_c(\mathbf{k})+\varepsilon_c(\mathbf{k}_1)-\varepsilon_c(\mathbf{k}')-\varepsilon_v(\mathbf{k}_f)). \quad (1)$$

Here, h is the Planck's constant, ($\mathbf{k}_1$, s_1), ($\mathbf{k}'$, s') are the wavevectors and quantum numbers of the second electron before ("cold") and after ("hot") recombination, respectively, and ($\mathbf{k}_f$, s_f) are the wavevector and quantum number of destination electronic state in the valence band. Note that $\mathbf{k}_f$ can be expressed as $\mathbf{k}_f = \mathbf{k}+\mathbf{k}_1-\mathbf{k}'$ due the momentum conservation law. Furthermore, $\epsilon_c(k)$ and $\epsilon_v(k)$ are the dispersion curves in the conduction and valence bands, $f(\mathbf{k}, s)$ is the Fermi-Dirac electron distribution function, and V is the matrix element of electron–electron interaction. For normalization purposes, we introduce the QW area S. With the z axis chosen to be perpendicular to the QW plane, electron wave functions can be expressed as $\Psi(\mathbf{k}, s, \mathbf{r}) = \exp(i\mathbf{k}\boldsymbol{\rho})\psi_s(\mathbf{k}, z)/\sqrt{S}$, where $\boldsymbol{\rho}$ is the radius-vector lying in the QW plane, and expression for V becomes

$$V(\mathbf{k},s,\mathbf{k}_1,s_1,\mathbf{k}',s',\mathbf{k}_f,s_1')=\int d\mathbf{r}d\mathbf{r}_1\Psi^+(\mathbf{k}',s',\mathbf{r})\Psi^+(\mathbf{k}_f,s_1',\mathbf{r}_1)U(\mathbf{r},\mathbf{r}_1)\Psi(\mathbf{k},s,\mathbf{r})\Psi(\mathbf{k}_1,s_1,\mathbf{r}_1)-\int d\mathbf{r}d\mathbf{r}_1\Psi^+(\mathbf{k}',s',\mathbf{r})\Psi^+(\mathbf{k}_f,s_1',\mathbf{r}_1)U(\mathbf{r},\mathbf{r}_1)\Psi(\mathbf{k},s,\mathbf{r}_1)\Psi(\mathbf{k}_1,s_1,\mathbf{r}). \quad (2)$$

Here, U is the potential of the screened Coulomb interaction, and first and second terms in (2) account for direct (V_d) and exchange (V_{ex}) electron–electron interaction, respectively.

To simplify the calculations, we neglect the difference between the dielectric constants of the quantum well and barriers. We also apply the approximation of a thin quantum well while evaluating electron–electron interaction, so that the QW thickness is less than

the average distance between interacting particles. Under these assumptions, we obtain the following expression for the matrix element of direct and exchange e–e interactions:

$$V_d(\mathbf{k}, s, \mathbf{k}_1, s_1, \mathbf{k}', s', \mathbf{k}_f, s_1') = \frac{2\pi e^2}{S\kappa}\int dz dz_1 \frac{\exp(-|\mathbf{k}-\mathbf{k}'||z-z_1|)}{(|\mathbf{k}-\mathbf{k}'|+1/\lambda)} \times \psi^+_{s'}(\mathbf{k}', z)\psi^+_{s_f}(\mathbf{k}_f, z_1)\psi_s(\mathbf{k}, z)\psi_{s_1}(\mathbf{k}_1, z_1), \quad (3a)$$

$$V_{ex}(\mathbf{k}, s, \mathbf{k}_1, s_1, \mathbf{k}', s', \mathbf{k}_f, s_1') = \frac{2\pi e^2}{S\kappa}\int dz dz_1 \frac{\exp(-|\mathbf{k}-\mathbf{k}'||z-z_1|)}{(|\mathbf{k}-\mathbf{k}_f|+1/\lambda)} \times \psi^+_{s'}(\mathbf{k}', z)\psi^+_{s_f}(\mathbf{k}_f, z_1)\psi_s(\mathbf{k}, z_1)\psi_{s_1}(\mathbf{k}_1, z). \quad (3b)$$

In the above expressions, e is the electron charge, κ is the dielectric constant, and λ is the characteristic screening length given by

$$1/\lambda = \frac{2\pi e^2 a}{\kappa}. \quad (4a)$$

If electrons and holes occupy only the lowest conduction and upper valence quantization subbands, respectively, the expression for a has the form

$$a = \frac{2}{(2\pi)^2 k_B T}\int d^2k \left\{ \frac{\exp\left(\frac{\varepsilon_c(k)-F_c}{k_BT}\right)}{\left[1+\exp\left(\frac{\varepsilon_c(k)-F_c}{k_BT}\right)\right]^2} + \frac{\exp\left(\frac{F_v+\varepsilon_v(k)}{k_BT}\right)}{\left[1+\exp\left(\frac{F_v+\varepsilon_v(k)}{k_BT}\right)\right]^2} \right\}, \quad (4b)$$

where T is the temperature, k_B is the Boltzmann constant, F_c and F_v are the electronic chemical potentials in the conduction and valence bands.

After the Auger recombination probability has been calculated, one can find the net recombination rate R_{Auger} from

$$R_{Auger} = \frac{1}{2}\sum_{k,s} W(k, s)f(k, s), \quad (5)$$

with the ½ factor accounting for the double summing of the same electrons in (5) and (1).

Note that we use a classical model to evaluate screening length, which greatly facilitates further calculations. A similar approach has been extensively used in preceding works (see, e.g., Refs. 3 and 8). The random-phase approximation (RPA)[9] is generally required to account for screening effects. For relatively wide-gap structures and low carrier densities, the transferred momentum exceeds the inverse screening length and screening effects are of minor importance. In the case of high carrier density and narrower gap HgCdTe QWs application of the classical model results in somewhat stronger screening (compared to RPA) while keeping all essential effects and tendencies, as it will be discussed below. Thus, we find our approach to be reasonable when drawing the general guidelines on optimizing the QW for lasing.

EXPERIMENTAL MEASUREMENT OF AUGER LIFETIME

In order to verify the adequacy of our model for Auger recombination, we simulated the interband photoconductivity (PC) kinetics and compared the calculated curve with the experimentally observed one. We performed our PC experiments on the sample with five 7.8 nm-thick $Hg_{0.92}Cd_{0.08}Te$ QWs separated by $Cd_{0.65}Hg_{0.35}Te$ barrier layers, grown on a [013] GaAs substrate (see Ref. 10 for details on the sample growth). Photoconductivity was excited by a tunable parametric light generator (Solar Laser Systems, Minsk, Belarus) operating at 9.5 μm wavelength. Investigated sample mounted in a liquid nitrogen Dewar at T = 77 K; excitation light was guided to the sample using a hollow metallic waveguide. The PC signal was passed through a 400 MHz current preamplifier and recorded using a digital oscilloscope (LeCroy 7100A). The temporal resolution of the setup was limited to 7 ns due to the excitation pulse duration. The PC setup is thoroughly described in Ref. 11.

Measured dynamics of the photoconductivity response is shown in Fig. 1. The PC signal was observable with reasonable accuracy up to about 300 ns delay after the excitation pulse (by this point, the PC dropped by a factor of 25 with respect to its initial value). We simulate the photoconductive response under the assumption that modulation of sample conductivity is directly proportional to the excess carrier density n. The latter value changes

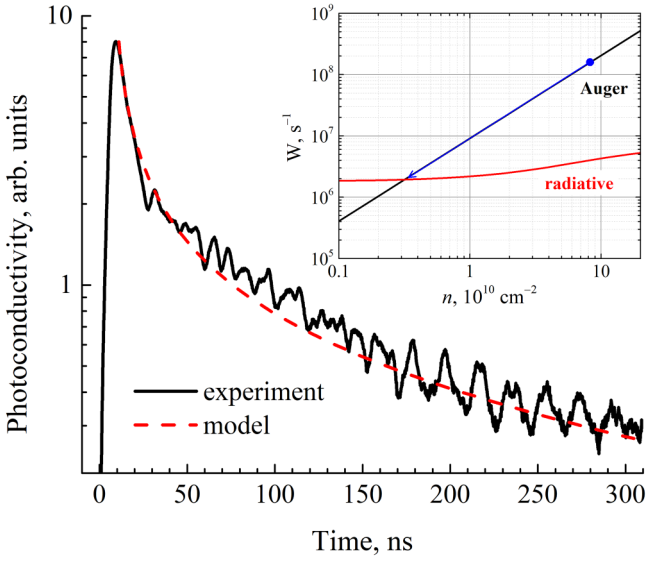

FIG. 1. Measured photoconductivity kinetics (solid black) and its model simulation (dashed red line). In the inset: probability of Auger recombination (black) and radiative recombination (red) depending on the excess carrier concentration. Arrow indicates the instant recombination rate as the excess carrier concentration decreases after the excitation pulse.

according to the balance equation

$$\frac{dn}{dt} = -R_{Auger} - R_{rad}, \tag{6}$$

which accounts for Auger recombination (R_{Auger}) and radiative processes (R_{rad}). Here, we point out that stimulated emission in the sample under consideration could not be achieved at temperatures above $T_{\max} \sim 50$ K, so we only consider spontaneous light emission at $T = 77$ K and calculate R_{rad} using the technique described in Ref. 12. Direct numerical integration of (6) gives the PC(t) dependence. Since the sample was mounted at the end of the long waveguide insert, estimation of the incident excitation flux was complicated. Therefore, the initial photocarrier density $n_{t=0}$ was considered a fitting parameter. The best agreement between the experimental and calculated PC traces is observed for $n_{t=0} = 8.5 \times 10^{10}$ cm^{-2} (see Fig. 1).

Note that the decay of the PC signal is determined by Auger (and not radiative) recombination over the entire interval of observation. The inset in Fig. 1 shows calculated dependencies of the average Auger and radiative recombination time on the excess carrier density. Starting at excess carrier concentration of $n_{t=0} = 8.5 \times 10^{10}$ cm^{-2}, Auger recombination is about two orders of magnitude faster than radiative processes; it is only at the final stages of photoconductivity relaxation the probability of radiative recombination becomes comparable to that of Auger recombination. It should be noted that it is not common for HgCdTe QW studied before: the carrier relaxation is most frequently strongly influenced or even determined by Shockley–Read–Hall[13] or radiative recombination.[12] Given good agreement between experimentally measured PC relaxation kinetics and simulated one, we conclude that our model is adequate for describing recombination processes in CdHgTe QWs.

AR AND RR RATES IN QW STRUCTURES FOR THE FAR-IR RANGE

Having approved the calculation technique in the previous section, we now apply it to the analysis of the QW designs most suitable for lasing in the far-infrared range. Here, we consider a series of QWs with identical bandgap energies of 40 meV (which corresponds to about 30 μm emission wavelength) while varying the QW composition (0%–9% Cd) and, accordingly, the QW thickness (see Table I for details). For all the QWs studied, we keep barrier layers at $Cd_{0.7}Hg_{0.3}Te$ composition, seemingly close to the optimal point, which balances between higher energy threshold E_{th} for the Auger recombination (higher Cd_{barr} fraction leads to higher E_{th}) and overall growth quality (which is generally better at lower Cd_{barr} values). Within this series, we calculate and compare low-temperature radiative and Auger recombination rates depending on the concentration of excess carriers.

TABLE I. The QW designs considered for far-IR lasing: d_{QW} and $[\mathrm{Cd}]_{\mathrm{QW}}$ are the well thickness and cadmium fraction, respectively (both are varied in the way that the bandgap E_g is fixed at 40 meV for $T = 8$ K temperature); E_{th} is the calculated energy threshold for CCHC-type AR.

Sample	E_g (meV)	d_{QW} (nm)	$[\mathrm{Cd}]_{\mathrm{QW}}$ (%)	E_{th} (meV)
A	40	4.9	0	35.8
B		6.0	3	29.1
C		7.9	6.5	19.8
D		10.1	9	12.9

Electronic spectra of the QWs under discussion, calculated at the temperature $T = 8$ K, are presented in Fig. 2. One can see that band dispersion remains almost unchanged in the vicinity of the Brillouin zone Γ-point as the cadmium fraction in the QWs increases. However, strong changes can be observed in the valence band dispersion at high k-values with cadmium admixture leading to the appearance of the pronounced side extrema. Such a behavior of hole dispersion curves is well established for HgCdTe/CdHgTe QWs (see, for example, Ref. 12).

Calculated radiative and Auger recombination rates are plotted in Fig. 3 depending on the excess carrier density. For the radiative processes, recombination rate increases initially with the excess carrier density until it reaches saturation due to phase space filling. However, further increase in the carrier concentrations leads to a decline in the average recombination rate: excess holes start to fill the side extrema in the valence band and cannot recombine radiatively[12] due to the absence of electrons with correspondingly large momentum. The effect is stronger and set in earlier for the QWs with higher Cd content which can be predicted from the band dispersion in Fig. 2.

Energy separation between main and side maxima decreases by a factor of 5.5 (33–6 meV) for Cd fraction in the QWs increasing from 0% to 9% and thus filling of the side maxima by the excess holes with increase in either carrier concentration or temperature seems to be detrimental for light emission from Cd-rich QWs. Interestingly, we calculated the interband dynamic conductivity for our QW designs and found that all of the QWs A

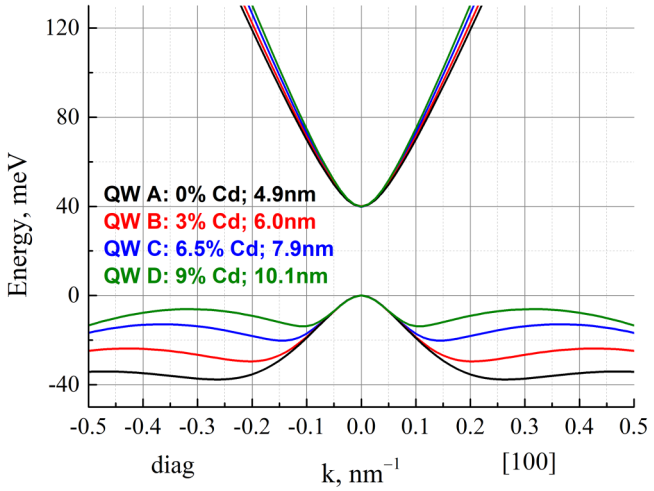

FIG. 2. Electronic spectra of the QWs studied, calculated for $T = 8$ K temperature. Band dispersion appears to be slightly anisotropic, so [100] and diagonal (between [100] and [03−1]) directions are shown.

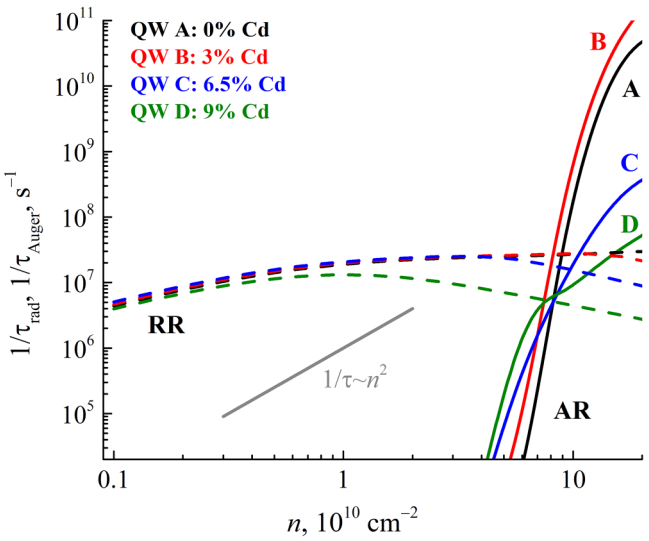

FIG. 3. Concentration dependences of the radiative (RR, dashed lines) and Auger (AR, solid lines) recombination rates for the QWs under consideration (see Table I). All calculations were performed for $T = 8$ K.

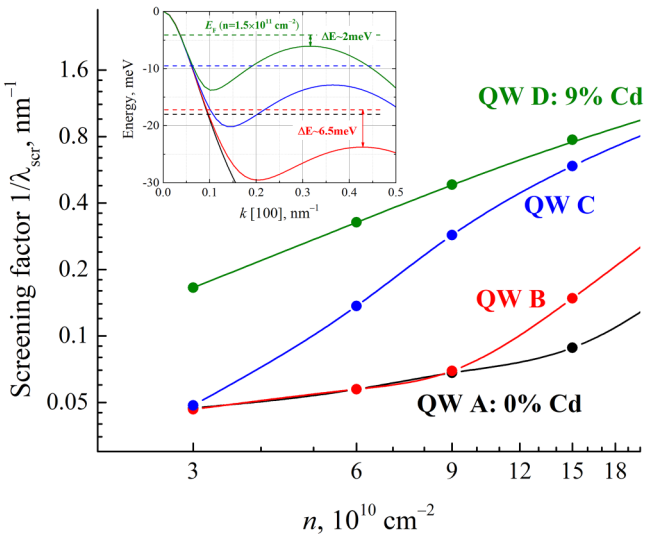

FIG. 4. Inverse screening length depending on the carrier concentration. Calculations for $T = 8$ K temperature for QW with 0/9% Cd content (see Table I). In the inset: position of Fermi level for holes relative to side maxima in the hole dispersion for samples A–D (at $T = 8$ K and $n = 1.5 \times 10^{11}$ cm^{-2}).

through D provided similar possible optical gain at realistic carrier concentrations (up to a few 10^{11} cm^{-2}). This result is attributed to the similarity of the band structure in the vicinity of the Γ-point and we suggest it only holds at low temperatures close to that of liquid helium. However, a strong upper bound for the cadmium content in the QWs does certainly exist since at [Cd] fraction above 10% electronic band structure switches rapidly toward indirect gap (at about 12% Cd), which is clearly unsuitable for lasing applications.

Given the above considerations, one may conclude that nonradiative recombination rate emerges as the only major factor which determines the optimal QW design within our series. Speaking in terms of Auger threshold energy, pure binary QWs seem to be unchallenged (see corresponding E_{th} values in Table I); however accurate microscopic calculations of the Auger recombination rate presented in Fig. 3 show that the correct answer is not so obvious. Note that calculated dependencies of the Auger recombination rate ($1/\tau_{Auger}$) on the carrier concentration n differ strongly from the $\sim n^2$ behavior (also marked in Fig. 3) which could be expected for a three-particle process with Maxwellian carrier statistics. It is only at very high concentrations (>10^{11} cm^{-2}) that Auger rate approaches the n^2-law. Two key factors contribute here into the effective Auger rate, first being the degeneracy of the electron gas and second – the screening of Auger (Coulomb) interaction by free charge carriers. The degeneracy of the electrons and holes is directly responsible for the rapid drop in the non-radiative recombination toward lower concentrations.

While Auger-rate is generally comparable with the radiative recombination rate at carrier concentrations of about $(7–8) \times 10^{10}$ cm^{-2}, it becomes negligible below $(4–5) \times 10^{10}$ cm^{-2}. We should point out that for $n < 7 \times 10^{10}$ cm^{-2} calculated curves arrange themselves according to the Cd fraction in the QWs, with Cd-low QWs exhibiting lower AR rates. This feature can be explained by the better overlap of the electron and hole wavefunctions in wider (Cd-rich) QWs, which leads to an increase in the interaction matrix element (2). Apparently, this is the reason why QWs with a Cd fraction of 3% (design B) retain a higher probability of Auger recombination compared to 0% Cd QWs (A) at any carrier concentration. On the contrary, QW designs C and D feature strongly suppressed AR (compared to A and B) at higher carrier concentrations, $n > 10^{11}$ cm^{-2}. We attribute it to the onset of the screening of Coulombic interaction by free holes.

Let us discuss screening effects in more detail in attempt to reveal the physics behind the non-intuitive dependence of Auger rates on Cd content in the QW. As can be seen from Fig. 2, the side maxima in the valence band have higher density of states than the region near the k = 0 point. Therefore, holes in the side maxima can introduce much stronger screening compared to the holes near the top of the valence band. At the same time, the side maxima are much closer to the valence band edge for Cd-rich QWs. Thus, the differences between structures are related to filling of side maxima in the valence bands with excess holes. Figure 4 shows calculated inverse screening length depending on the carrier concentration for the QWs under study. One can see that screening is much more pronounced for samples D and C than for samples B and A in a relevant concentration range. With increasing carrier concentration, hole Fermi level (refer to the inset in Fig. 4 for Fermi levels calculated at $n = 1.5 \times 10^{11}$ cm^{-2}) moves down into the valence band until it approaches the top of side maxima where it stabilizes due to a very high density of states in the side maxima compared to those of main the maximum at $k = 0$. At this point, screening becomes the most efficient since it is determined by the

number of holes distributed in the vicinity of Fermi level. Thus, characteristic carrier density corresponding to the turn-on of screening roughly corresponds to the "capacity" of the main maximum before side bands start populating noticeably (including thermal broadening of the distribution function at finite temperatures; $k_BT \sim 0.7$ meV at $T = 8$ K). Consequently, for QWs with lower Cd fraction (A and B), screening effects are relatively weak at practical carrier densities and do not vary strongly with increasing concentration, while for QW D screening is an important issue even at carrier density as low as $n \sim 3 \times 10^{10}$ cm^{-2}. To provide some quantitative reference, we have calculated Auger rates for samples with pure HgTe QW (A) and 6.5% Cd QW (C) at carrier concentration $n = 1.5 \times 10^{11}$ cm^{-2} without screening. For QW A, which is expected to be relatively insensitive to screening, the resulting "unscreened" AR rate was 4×10^{10} s^{-1} compared to 1.3×10^{10} s^{-1} obtained with screening taken into account, with a suppression factor of about 3 only. Conversely, we expect strong screening in sample C at $n = 1.5 \times 10^{11}$ cm^{-2} and corresponding values of "unscreened" and "screened" Auger recombination rates were calculated at 5.4×10^{9} s^{-1} and 1.5×10^{8} s^{-1}. Thus, in Cd-rich QWs strong screening of the Coulomb interactions leads to suppression of AR by a factor of more than 30 and so we expect QWs with a moderate Cd fraction of 6%–9% (and not pure HgTe QWs) to provide the best performance for far-IR lasing. In such QWs Auger recombination is suppressed at high concentrations of excess carriers, up to 10^{11} cm^{-2}. It may be extremely important since activation of Auger processes inevitably heats the electron gas in the QWs, which further increases the AR rate.

Finally, we should mark certain reference points for the practical carrier concentrations in the HgCdTe/CdHgTe QWs under study. First, the calculated transparency concentration for our QWs is about 5×10^{9} cm^{-2}, taking into account interband conductivity and free-carrier absorption. This concentration is far below any margin where Auger recombination may start to appear, and radiative recombination should dominate. However, there is also a factor of phonon-related cavity losses, which depends strongly on the waveguide design and on the particular lasing wavelength since the lattice absorption changes rapidly across the wavelength in the region of interest due to both single- and two-phonon processes.[14] At the local absorption minimum around 30–32 μm wavelength, excess carrier concentration of about 5×10^{10} cm^{-2} is required to overcome phonon losses, which is actually close to the crossover point between radiative- and Auger-dominated regions. Further increase in carrier concentration may provide lasing either at elevated temperatures or in the spectral regions with higher lattice absorption; these estimates are beyond the scope of the present work. Thus, the relevant range of threshold carrier density n_{th} (i.e., density required for lasing) lies from 10^{10} cm^{-2} to several units of 10^{11} cm^{-2} depending on resonator properties and losses. There is however a strong limiting factor for a practically attainable carrier density: in narrow-gap QWs interband recombination with the emission of two-dimensional plasmons may become dominant recombination channel at sufficiently high concentrations of excess carriers.

Recombination of excess carriers with emission of 2D plasmons in HgTe QWs was discussed in detail in Ref. 15. In this work, we apply the model developed in Ref. 15 to evaluate whether such a mechanism competes with radiative and Auger-processes.

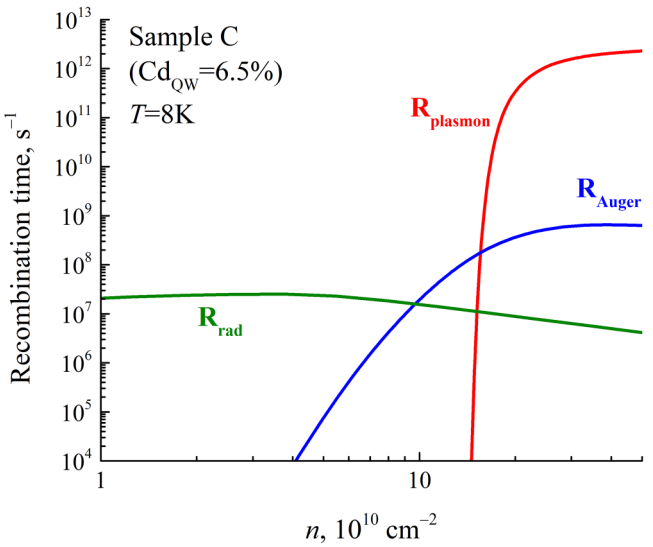

FIG. 5. Comparison of the radiative (R_{rad}), Auger (R_{Auger}) and plasmon-assisted ($R_{plasmon}$) recombination rates for QW design C (6.5% Cd fraction in the QW) depending on the concentration of excess carriers. All data calculated for $T = 8$ K.

To be specific, we consider a 6.5% Cd-content HgCdTe QW (sample C, Table I); the result of our calculations is shown in Fig. 5. Plasmon-assisted appears to be extremely efficient (with characteristic relaxation times at a ps-scale) with a very sharp onset once the carrier concentration reaches a certain threshold value. This threshold can be explained as follows: since plasmon carries away finite momentum, plasmon-assisted recombination is essentially an indirect-k process which relies on the presence of holes with substantial momentum/energy.[16] For the QW under analysis, threshold concentration for a plasmon-assisted process is approximately 1.5×10^{11} cm^{-2}. The above value poses a solid upper limit for the excess carrier density in our QWs under any reasonable excitation conditions. Note also that the effective refractive index for the 2D plasmons in our QW heterostructures exceeds 100. Therefore, generated plasmons are being back-reflected at the sample boundaries and cannot efficiently leave the active layer. In this case the energy released upon subsequent plasmon recombination will be spent on heating the electron and hole gases which will prevent the realization of the inverted population of the bands and stimulated generation of plasmons unless special efforts are taken for plasmon outcoupling, similar to Ref. 16.

CONCLUSIONS

To summarize, we developed a microscopic model to calculate Auger recombination rates in narrow-gap HgCdTe/CdHgTe QWs with consideration to complex band dispersions and wavefunctions in the QWs, degenerate carrier statistics and screening effects. We also directly demonstrate the carrier relaxation controlled only by the Auger process in experiments for a HgCdTe QW. It is shown to be consistent with previous experimental data on

stimulated emission, and the experimental curve is well described by our theoretical model.

Then, we apply our model to evaluate Auger rates in a series of samples with a bandgap of 40 meV while varying Cd content in the QWs. For low-threshold lasing ($n_{th} < 8 \times 10^{10}$ cm^{-2}) opting out the structure with a maximum threshold energy for the Auger process proves to be reasonable, resulting in pure binary HgTe QWs as the optimal choice. According to our calculations, at high carrier concentrations cadmium-enriched (6%–9% Cd) HgCdTe QWs can feature reduced Auger recombination rates in spite of lower "threshold energy" for the Auger process than that in cadmium-free binary HgTe QWs. The mitigation of Auger process results from stronger screening of Coulomb interaction by free charge carriers in the side maxima of the valence band. Though the absolute values of Auger lifetimes are probably to be adjusted using more elaborate model, this effect is directly related to a higher density of states in the side maxima and therefore is fundamental. Thus, HgCdTe with a moderate cadmium fraction may be the preferable QW material to realize far-infrared lasing in structures where $n_{th} \sim 10^{11}$ cm^{-2} and higher.

ACKNOWLEDGMENTS

This work was supported by the Ministry of Science and Higher Education of the Russian Federation (World-Level Research Center program, Agreement No. 075-15-2020-906). The authors thank D. Svintsov (Moscow Institute of Physics and Technology) for proofreading of the manuscript.

DATA AVAILABILITY

The data that support the findings of this study are available from the corresponding author upon reasonable request.

REFERENCES

[1]S. V. Morozov, V. V. Rumyantsev, M. A. Fadeev, M. S. Zholudev, K. E. Kudryavtsev, A. V. Antonov, A. M. Kadykov, A. A. Dubinov, N. N. Mikhailov, S. A. Dvoretsky, and V. I. Gavrilenko, Appl. Phys. Lett. **111**, 192101 (2017).
[2]G. Alymov, V. Rumyantsev, S. Morozov, V. Gavrilenko, and D. Svintsov, ACS Photonics **7**, 98 (2020).
[3]Y. Jiang, M. C. Teich, and W. I. Wang, J. Appl. Phys. **69**, 6869 (1991).
[4]I. Vurgaftman and J. R. Meyer, Opt. Express **2**, 137 (1998).
[5]M. S. Vitiello, G. Scalari, B. Williams, and P. De Natale, Opt. Express **23**, 5167 (2015).
[6]M. Zholudev, Ph.D. thesis (University Montpellier 2, France), 2013.
[7]V. Ya. Aleshkin, A. A. Dubinov, S. V. Morozov, and V. V. Rumyantsev, J. Phys.: Condens. Matter **31**, 425301 (2019).
[8]F. Rana, Phys. Rev. B **76**, 155431 (2007).
[9]J. Lindhard, Kgl. Danske Videnskab. Selskab, Mat.-Fys. Medd. **28**, N8 (1954)
[10]S. Dvoretsky, N. Mikhailov, Yu. Sidorov, V. Shvets, S. Danilov, B. Wittman, and S. Ganichev, J. Electron. Mater. **39**, 918 (2010).
[11]P. A. Bushuykin, B. A. Andreev, V. Yu. Davydov, D. N. Lobanov, D. I. Kuritsyn, A. N. Yablonskiy, N. S. Averkiev, G. M. Savchenko, and Z. F. Krasilnik, J. Appl. Phys. **123**(19), 195701 (2018).
[12]V. Ya. Aleshkin, A. A. Dubinov, V. V. Rumyantsev, M. A. Fadeev, O. L. Domnina, N. N. Mikhailov, S. A. Dvoretsky, and S. V. Morozov, J. Phys.: Condens. Matter **30**, 495301 (2018).
[13]V. V. Rumyantsev, M. A. Fadeev, S. V. Morozov, A. A. Dubinov, K. E. Kudryavtsev, A. M. Kadykov, I. V. Tuzov, S. A. Dvoretskii, N. N. Mikhailov, V. I. Gavrilenko, and F. Teppe, Semiconductors **50**, 1654 (2016).
[14]J. Polit, Bull. Pol. Acad. Sci.: Tech. Sci. **59**(3), 331 (2011).
[15]V. Ya. Aleshkin, G. Alymov, A. A. Dubinov, V. I. Gavrilenko, and F. Teppe, J. Phys. Commun. **4**, 115012 (2020).
[16]K. Kapralov, G. Alymov, D. Svintsov, and A. Dubinov, J. Phys.: Condens. Matter **32**, 065301 (2020).